12-2014

Split-step Approach to Electromagnetic Propagation through Atmospheric Turbulence using the Modified von Karman Spectrum and Planar Apertures

Monish Ranjan Chatterjee
University of Dayton, mchatterjee1@udayton.edu

Fathi H.A. Mohamed
University of Dayton

Optical Engineering

OpticalEngineering.SPIEDigitalLibrary.org

Split-step approach to electromagnetic propagation through atmospheric turbulence using the modified von Karman spectrum and planar apertures

Monish R. Chatterjee
Fathi H. A. Mohamed

SPIE.

Split-step approach to electromagnetic propagation through atmospheric turbulence using the modified von Karman spectrum and planar apertures

Monish R. Chatterjee* **and Fathi H. A. Mohamed**
University of Dayton, Department of Electrical and Computer Engineering, 300 College Park, Dayton, Ohio 45469, United States

Abstract. The impact of atmospheric phase turbulence on Gaussian beam propagation along propagation paths of varying lengths is examined using multiple random phase screens. The work is motivated by research involving generation and encryption of acousto-optic chaos, and the interest in examining propagation of such chaotic waves through atmospheric turbulence. A phase screen technique is used to simulate perturbations to the refractive index of the medium through the propagation path. A power spectral density based on the modified von Karman spectrum model for turbulence is used to describe the random phase behavior of the medium. In recent work, results for the numerical simulation of phase turbulence over a narrow region of space implemented by placing a planar aperture representing a (narrow) random phase screen were presented. Results are presented pertinent to extended phase screens (via multiple random-phase apertures) through which an incident Gaussian beam propagates incrementally via alternate phase transmission and diffraction along the propagation path. Additionally, for profiled electromagnetic waves (such as Gaussian), the scintillation index is evaluated for extended phase turbulence, and finally, fringe visibility due to the interference of double-Gaussian beams passing through extended turbulence is examined. [DOI: 10.1117/1.OE.53.12.126107]

Keywords: atmospheric turbulence; Gaussian beam; modified von Karman spectrum; scintillation index; fringe visibility; narrow and extended phase turbulence.

Paper 141429P received Sep. 12, 2014; accepted for publication Nov. 4, 2014; published online Dec. 11, 2014.

1 Introduction

It is known that as an electromagnetic (EM) wave propagates through the atmosphere, turbulence induces amplitude and phase fluctuations. Atmospheric turbulence has been a subject of study for many years, and there is a wide interest in applications that consider effects of atmospheric turbulence on optical systems.[1] The foundations of the study of atmospheric turbulence were laid in the late 1960s and 1970s even though the field may be traced to many decades earlier. A vast amount of work regarding propagation through atmospheric turbulence is available in the literature. In several cases, turbulence is modeled via random phase screens that are either localized or extended over a physical space representing the turbulent medium.[2–4] Some of the commonly used models include the Kolmogorov, Tatarski, von Karman, and modified von Karman.[3,5] The phase fluctuations of the phase screen used to model the random phase distribution within the aperture are parameterized by the Fried parameter, which describes the transverse coherence length, and the inner and outer scales that determine the amount of aberration seen by the propagating beam. In addition, the split-step beam propagation method (SSBPM) with the Fresnel–Kirchhoff diffraction integral is used to model the propagation of the EM through turbulence media.

In our initial approach to represent atmospheric turbulence, we were motivated by recent work involving generation of acousto-optic (AO) chaos and utilization of such chaos in encrypting the chaotic carrier with RF information signals, which were then transmitted and subsequently recovered using a set of matched keys (system parameters).[6–9] It has been suggested[10] that the propagation of a chaotic wave through turbulence may offer certain immunizing properties that would make the propagated signal relatively undisturbed by the turbulence in the medium. In pursuing this goal, the problem was set up by means of a thin, random phase screen representing turbulent phase fluctuations in a thin layer of the medium (along the lines of the modified von Karman phase model, which is used throughout this work). Thereafter, profiled input EM waves would be transmitted over a fixed distance along the propagation path. The simulation and numerical analysis of this problem eventually led to the finding that this approach which includes the use of an SSBPM involving the Fresnel–Kirchhoff diffraction integral whereby the EM wave alternately moves through a random-phase layer and then a thin layer of pure diffraction may be used conveniently as a good model simply to study both near- and far-field diffractions through arbitrary apertures and involving profiled EM beams, with and without atmospheric turbulence, and also with and without the use of the split-step algorithm. At this stage, we need to point out that beyond the turbulence simulation presented here (using the split-step approach instead of other methods), which admittedly has been analyzed by several other researchers via both analytical and field measurements.[11,12] A broader goal for this work (which is continuing at the moment) as

*Address all correspondence to: Monish R. Chatterjee, E-mail: mchatterjee1@udayton.edu

0091-3286/2014/$25.00

mentioned before is to investigate the signal propagation characteristics for chaotic EM waves (with or without modulation) propagating through different types of turbulence, specifically the modified von Karman spectrum (MVKS)-type as discussed in this paper.

In this paper, we have studied the effect of the atmospheric turbulence on the propagation of the Gaussian beam profile. Some of the salient characteristics of EM propagation through turbulence involving atmospheric channel effects and free-space laser communications have been discussed in Ref. 13. Two scenarios are followed in this paper, (a) single-random phase screen where the random phase screen is located at a particular distance from the aperture plane then the field intensity at the observation (image) plane is calculated, and (b) extended (multiple) random phase screens whereby a certain number of random phase screens are placed in equally infinitesimal distance (Δz) and then the field intensity at different positions and at the image plane is also calculated. In both scenarios, three parameters are chosen in this work, (a) strength of turbulence (weak and strong), (b) propagation distance, and (c) Δz for extended phase screen. More details about theses parameters will be discussed in the simulation results and interpretation. Also, some work regarding time statistical in atmospheric turbulence is done where a single-random phase screen is located at a certain distance and the amplitude and phase of the field intensity at the image plane are computed. Moreover, an SSBPM is used whereby either a single (narrow) random phase screen or extended (multiple) random phase screens are placed at arbitrary location(s) along the propagation path. The work reported here also includes the results of some additional investigations. The scintillation index (SI) of Gaussian beam propagation through extended turbulence as well as the fringe visibility (FV) due to interference between a twin set of Gaussian beams propagating through extended turbulence are also calculated.

The organization of this paper is as follows: In Sec. 2, the power spectrum models for refractive index fluctuations, the MVKS, Fried parameter, SI, and FV are discussed. General methodologies for modeling propagation through narrow and extended turbulent media are outlined in Sec. 3. Simulation results and interpretations for the different cases are reported in some detail in Sec. 4. Finally, concluding remarks and ideas to further expand the research are presented in Sec. 5.

2 Power Spectrum Models for Refractive Index Fluctuations

The index of refraction is one of the most significant parameters of the atmospheric for optical wave propagation. The index of refraction of the atmosphere, $n(\vec{r})$, is modeled as the sum of a mean index of refraction, n_0, and a randomly fluctuating term, $n_1(\vec{r})$:[14]

$$n(\vec{r}) = n_0 + n_1(\vec{r}), \tag{1}$$

where $\vec{r}$ is a three-dimensional (3-D) vector position, $n_0 = n(\vec{r}) \approx 1$ is the mean value of the index of refraction of air, and $n_1(\vec{r})$ represents the random deviation of $n(\vec{r})$ from its mean value $[n_1(\vec{r}) = 0]$. Hence,

$$n(\vec{r}) = 1 + n_1(\vec{r}). \tag{2}$$

The statistical description of the random field of turbulence-induced fluctuations in the atmospheric refractive index is similar to that for the related random field of turbulent velocities. In particular, an inertial subrange is bounded by outer and inner scales, L_0, and ℓ_0, respectively. In this subrange, statistical properties of the refractive index are homogenous and isotropic.[14,15] The covariance function of $n(\vec{r})$ may be expressed by

$$B_n(\vec{r}_1, \vec{r}_2) = B_n(\vec{r}_1, \vec{r}_1 + \vec{r}) = n_1(\vec{r}_1) n_1(\vec{r}_1 + \vec{r}), \tag{3}$$

where $\vec{r}_1$ and $\vec{r}_2$ are two points in space, and $\vec{r} = \vec{r}_2 - \vec{r}_1$. Assuming a homogeneous and isotropic turbulent medium, the covariance function reduces to a function of only the scalar distance $\vec{r} = |\vec{r}_2 - \vec{r}_1|$. This may also be viewed as relative to a spatial or translational invariance.

Locally homogeneous fields are usually not characterized by the covariance function, but by the structure function defined as the mean-squared difference of the refractive index at two points:[14]

$$D_n(r) = [n(r_1 + r) - n(r_1)]^2 \ = 2[B_n(0) - B_n(r)]. \tag{4}$$

By substituting Eq. (3) into Eq. (4) and applying the well-known two-thirds law, we get the structure function of refractive index fluctuations for separations in the intermediate range between L_0 and ℓ_0:[14]

$$D_n(r) = C_n^2 \, r^{2/3}, \qquad \ell_0 \ll r \ll L_0, \tag{5}$$

where C_n^2 is the index of refraction structure parameter, also called the structure constant. C_n^2 typically ranges from 10^{-17} $\mathrm{m}^{-2/3}$ or less for conditions of "weak turbulence" to 10^{-13} $\mathrm{m}^{-2/3}$ or more when the turbulence is "strong."

The 3-D spatial power spectrum of the random field $\Phi_n(\vec{k})$ forms a 3-D Fourier transform pair with the covariance function:[16,17]

$$B_n(\vec{r}) = \iiint_{-\infty}^{\infty} e^{i\vec{k}\cdot\vec{r}} \Phi_n(\vec{k}) \mathrm{d}^3 k, \tag{6}$$

$$\Phi_n(\vec{k}) = \left(\frac{1}{2\pi}\right)^3 \iiint_{-\infty}^{\infty} e^{-i\vec{k}\cdot\vec{r}} \, B_n(\vec{r}) \mathrm{d}^3 r, \tag{7}$$

where $\vec{k}$ is the wave vector. Assuming homogeneity and isotropy, these Fourier transform relations reduce to their one-dimensional forms,

$$\Phi_n(\vec{k}) = \frac{1}{2\pi^2 k} \int_0^{\infty} B_n(r) \sin(kr) r \mathrm{d}r, \tag{8}$$

$$B_n(r) = \frac{4\pi}{r} \int_0^{\infty} \Phi_n(\vec{k}) \sin(kr) k \mathrm{d}k. \tag{9}$$

Consequently, the relation between the spectrum and structure function may be expressed by[14]

$$D_n(r) = 2[B_n(0) - B_n(r)] = 8\pi \int_0^\infty k^2 \Phi_n(\vec{k}) \left(1 - \frac{\sin(kr)}{kr}\right) \mathrm{d}k, \tag{10}$$

and

$$\Phi_n(\vec{k}) = \frac{1}{4\pi^2 k^2} \int_0^\infty \frac{\sin(kr)}{kr} \frac{\mathrm{d}}{\mathrm{d}r} \left[r^2 \frac{\mathrm{d}}{\mathrm{d}r} D_n(r)\right] \mathrm{d}r. \tag{11}$$

The correlation and covariance functions represent a spatial domain description whereas the power spectrum is a wave number representation.

2.1 *Modified von Karman Spectrum*

A turbulence model incorporating both the inner and outer scale parameters is the MVKS and has the form[14]

$$\Phi_n(k) = 0.033 C_n^2 \frac{e^{-\frac{k^2}{k_m^2}}}{(k^2 + k_o^2)^{\frac{11}{6}}}, \qquad 0 \le k \gg \infty, \tag{12}$$

where C_n^2 is the structure parameter mentioned before, k is the wave number, $k_m = 5.92/\ell_0$ is an equivalent unbounded wavenumber corresponding to the inner scale ℓ_0, and $k_o = 2\pi/L_0$ is an equivalent unbounded wavenumber corresponding to the outer scale L_0.

2.2 *Fried Parameter (r_0), Scintillation Index (SI), and Fringe Visibility (FV)*

The model used in subsequent sections relies heavily upon the Fried parameter. The Fried parameter and structure constant are intricately related; however, the structure constant is more frequently used. Thus, it is important not only to discuss the relation of the parameters but also the manner in which they affect the results obtained in our simulated models. The structure constant C_n^2 describes the index of refraction fluctuations and is used to characterize the strength of these fluctuations in the atmosphere. The Fried parameter describes the transverse coherence length, and the inner and outer scales. The relationship connecting the structure constant to the Fried parameter is as follows:[15]

$$r_0 = q \left[\frac{4\pi^2}{k^2 L C_n^2}\right]^{3/5}, \tag{13}$$

where q is a dimensionless quantity that is numerically 0.185 for plane waves and 3.69 for spherical waves, and L is the distance of propagation within the turbulence.

For free-space optical communications, it is important to understand the effects of atmosphere on propagating beams, because the atmosphere creates beam wander and scintillation. The SI quantifies the irradiance variance of an optical wave propagated through atmospheric turbulence. The SI is the "normalized variance of irradiance" and mathematically defined as[3]

$$\sigma^2(r, L) = \frac{\langle I^2(r, L)\rangle}{\langle I(r, L)\rangle^2} - 1, \tag{14}$$

where $\langle\,\rangle$ denotes the ensemble average for mean-square irradiance, while $\langle\,\rangle^2$ denotes the square of the mean, $I(r, L)$ is the local irradiance, L is the propagation distance of the beam, and r is the radial distance from the symmetry axis. The turbulence is weak if the SI is less than unity. Incidentally, power spectral models and their applications have been explored using alternative methods in Ref. 14.

For two identical Gaussian beams, separated by a given transverse spatial distance, the beams constructively and destructively interfere resulting in fringes as the beams propagate to the far-field. The contrast and quality of the fringes are generally a measure of the optical coherence and defined with a metric commonly referred to as FV. FV, mathematically defined in terms of the intensity on the observation plane, is given by

$$\mathrm{FV} = \frac{I_{\max} - I_{\min}}{I_{\max} + I_{\min}}. \tag{15}$$

In this paper, we measure FV for extended phase turbulence for weak and strong cases.

3 Propagation through Narrow and Extended Turbulence

In this section, we discuss the propagation of the EM waves through narrow and extended atmospheric turbulence. The SSBPM [also called the beam propagation method (BPM)] involving the Fresnel–Kirchhoff diffraction integral is applied for the study of the profiled beams across planar apertures and narrow or extended turbulence, along the lines used in an earlier paper.[18] The BPM is widely used for the numerical simulation of the propagation through many types of media: inhomogeneous, anisotropic, and nonlinear including waveguiding structures with weak variations along the propagation direction.[17]

3.1 *Propagation through Narrow Turbulence*

In this scenario, the propagation may be visualized as consisting of the passage of a profiled beam across a planar input aperture, followed by subsequent passage through a narrow region where turbulence occurs. The narrow turbulence, when modeled as a random phase fluctuation (as in the MVKS model), may be represented as a planar phase screen that may be placed anywhere between the aperture and the image plane, depending on the placement of the turbulence itself relative to the propagation. This is indicated in Fig. 1, where the phase screen has been placed at a distance L_1 from the aperture at $z = 0$, and the image plane is at $z = L$.

From Fig. 1, the total propagation distance is divided in two segments (L_1 and L_2), where $L = L_1 + L_2$. The EM beam first travels the longitudinal distance (L_1), which is free from turbulence. In this region, the field is subjected to the familiar Fresnel–Kirchhoff diffraction integral with z replaced by L_1 as follows:[19]

$$U(x_i, y_i) = \iint_{-\infty}^{\infty} U(x_o, y_o) e^{\left\{j\frac{k}{2z}[(x_i - x_o)^2 + (y_i - y_o)^2]\right\}} \mathrm{d}x_o \mathrm{d}y_o, \tag{16}$$

where $U(x_o, y_o)$ is the input (profiled) beam, $U(x_i, y_i)$ is the field after distance L_1, k is the unbounded wave number, and λ is the wavelength in the medium.

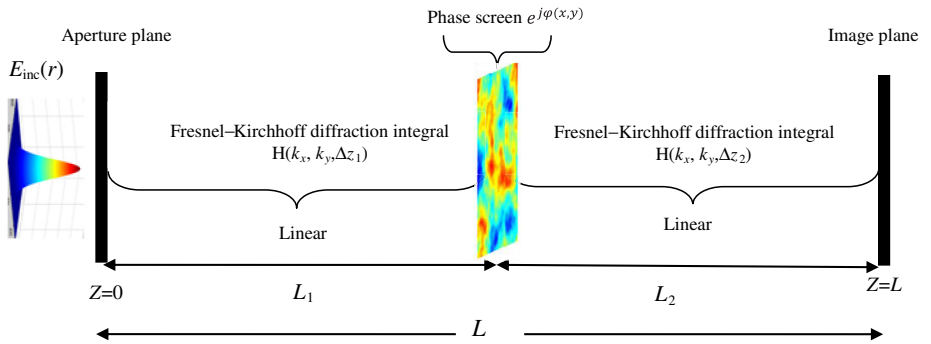

Fig. 1 Schematic illustration and physical interpretation of propagation through narrow turbulence.

The diffracted EM wave subsequently reaches the random phase screen defined by the MVKS model $[\Phi_n(k)]$ defined in the spatial frequency domain. It is then processed via a series of transformations so that we finally obtain a spatial phase distribution φ_{ij}, where the subscripts (i, j) imply spatial coordinates of points on the chosen grid within which the phase distribution is applied. Once the random phase screen representing MVKS turbulence has been generated, the wave is then transmitted through such a (planar) screen placed at $z = L_1$. The phase perturbations caused by refractive index fluctuations arising from MVKS turbulence across the planar phase screen may be represented by multiplying the input diffracted field by the phase function $e^{j\varphi(x,y)}$ as follows:

$$U_{out}(x_i, y_i) = U_{in}(x_i, y_i)\ e^{j\varphi(x_i, y_i)}, \tag{17}$$

where $U_{out}(x_i, y_i)$ is the field amplitude immediately after random phase screen, and $U_{in}(x_i, y_i)$ is the field before random phase screen. We note at this stage that narrow turbulence may be modeled via a single-phase screen placed at an appropriate position along the propagation path; likewise, extended or deep turbulence may be modeled using a series of planar phase screens along the propagation path. The latter modeling will be discussed further in Sec. 4. The propagation from L_1 to the image plane using the planar random screen therefore appropriately models the narrow turbulence along with associated Fresnel–Kirchhoff diffraction until the observation (or image) plane is reached.

3.2 *Propagation through Extended Turbulence*

The extended case (via multiple random phase screens) is an extension of narrow turbulence, where the propagation distance L is divided into arbitrarily small segments $\Delta z = L/n$, where n is an integer equal to the number of phase screens as illustrated in Fig. 2. The diffracted EM beam is propagated through subsequent narrow phase screens multiple times as needed, and the same procedure is applied as mentioned in the narrow turbulence case. All the simulation results presented in this paper were carried out using SSBPM either in the narrow or extended turbulence regime.

4 Numerical Simulation, Results, and Interpretations

In this section, we present numerical simulation results for profiled Gaussian beam propagation through a turbulent medium. Two scenarios are followed in this paper: the case of narrow turbulence represented by a planar phase screen is presented briefly, while that for extended turbulence is discussed at some length with more detail. Some of the parameters are kept constant during the simulation process. These parameters are: number of sample points (grid resolution) $=$ 512×512, wavelength $\lambda = 1\ \mu$m, physical size of grid $=$ 500 mm $\times$ 500 mm, inner scale $\ell_0 = 10$ mm;, and outer scale $L_0 = 1000$ mm, respectively. As we mentioned earlier, the other parameters (C_n^2 or r_0, L and Δz) are varied depending on whether the turbulence is weak or strong, and different propagation distances. In the extended turbulence case, additionally, the incremental distance Δz representing the physical distance between two adjacent phase screens has to be accounted for. We note here that the extended turbulence modeled here consists of multiple narrow turbulences spatially separated by Δz, which in our numerical simulations, is not necessarily infinitesimally small. This implies that the "extended" medium is idealized as narrow turbulences

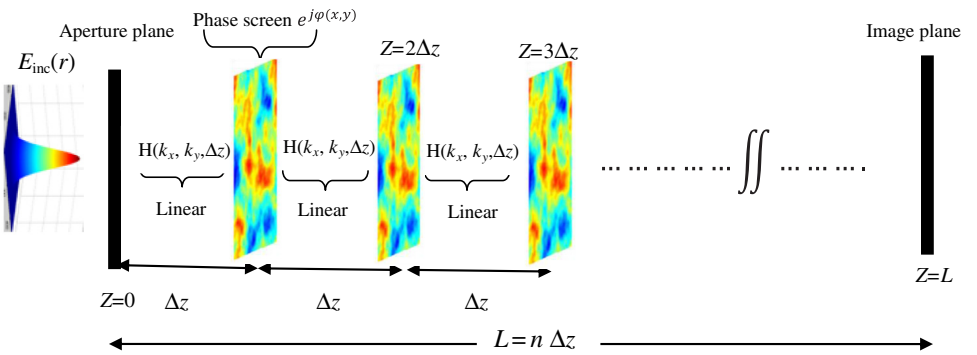

Fig. 2 Schematic illustration and physical interpretation of propagation through extended turbulence.

followed by short regions of pure diffraction and thereafter repeated multiple times. A true extended turbulence problem would require Δz to be arbitrarily small (likely smaller than the turbulence scale sizes); however, in many cases, the problem is analyzed with somewhat larger Δz values, thereby implying discretely separated turbulence. In this section, the SI of the propagated Gaussian beam for extended phase turbulence is also reported. Finally, some simulation results are presented by passing double-Gaussian beams through extended phase turbulence, and the FV at the observation plane is calculated.

4.1 *Narrow Turbulence through Single-Phase Screen*

As we mentioned above, the simulation results reported here use a narrow random phase screen placed at $z = 0$; the field is then evaluated at the image plane (at $z = L$). We limit the results to the strength of turbulence (weak and strong) and the propagation distance ($L = 1$ km and $L = 10$ km). The Gaussian beam 3-D view, its transverse plane intensity distribution, two-dimensional (2-D) intensity profile, the random phase screen distribution profile, and the field phase angle distribution in 3-D are evaluated at the image plane ($z = L$). The results are shown in the following figures.

4.1.1 *Turbulence strength*

Here, we use beam waist $w_0 = 50$ mm, and propagation distance is 5 km.

(a) Weak turbulence ($r_0 = 10$ mm or $C_n^2 = 1.067 \times 10^{-18}$ m$^{-2/3}$)

(b) Strong turbulence ($r_0 = 0.01$ mm or $C_n^2 = 1.067 \times 10^{-13}$ m$^{-2/3}$)

4.1.2 *Propagation distance (L)*

We consider moderate turbulence ($r_0 = 0.5$ mm):

(a) $L = 1$ km $C_n^2 = 7.8625 \times 10^{-16}$ m$^{-2/3}$

(b) $L = 10$ km $C_n^2 = 7.8625 \times 10^{-17}$ m$^{-2/3}$

In general, from the Figs. 3 and 4, we observe that the Gaussian beam suffers more distortion and higher phase fluctuations in the case of strong turbulence than for weak turbulence, as expected. Also, we observe that the propagated Gaussian beam tends to undergo profile splitting and other potential deformations under strong turbulence, as seen clearly in Fig. 4(c). Incidentally, the variance of the phase fluctuations in the image plane for weak turbulence turned out to be about 2 (implying a standard deviation of the phase of about 1.4 rad), whereas that for strong turbulence turned out to be about 4 (implying a standard deviation of about 2 rad). These statistical results indicate a higher degree of phase variations for strong turbulence. From Figs. 5 and 6, as the propagation distance increases (from 1 to 10 km), the intensity profile of the propagated Gaussian beam (at $z = L$) also broadens further (from $w_0 \approx 50$ mm to $w_0 \approx 82$ mm), respectively. Additionally, the intensity of the propagated beam (at $z = L$) is further attenuated (0.98 W/m^2 in case of 1 km and 0.38 W/m^2 in case of 10 km) as the propagation distance increases. We note that even though the peak of the intensity profile is lowered, the effective power under the Gaussian is conserved since the medium is assumed to be lossless.

4.2 *Extended Turbulence through Multiple Phase Screens*

We next consider passage of a profiled Gaussian beam through an extended turbulent medium represented by

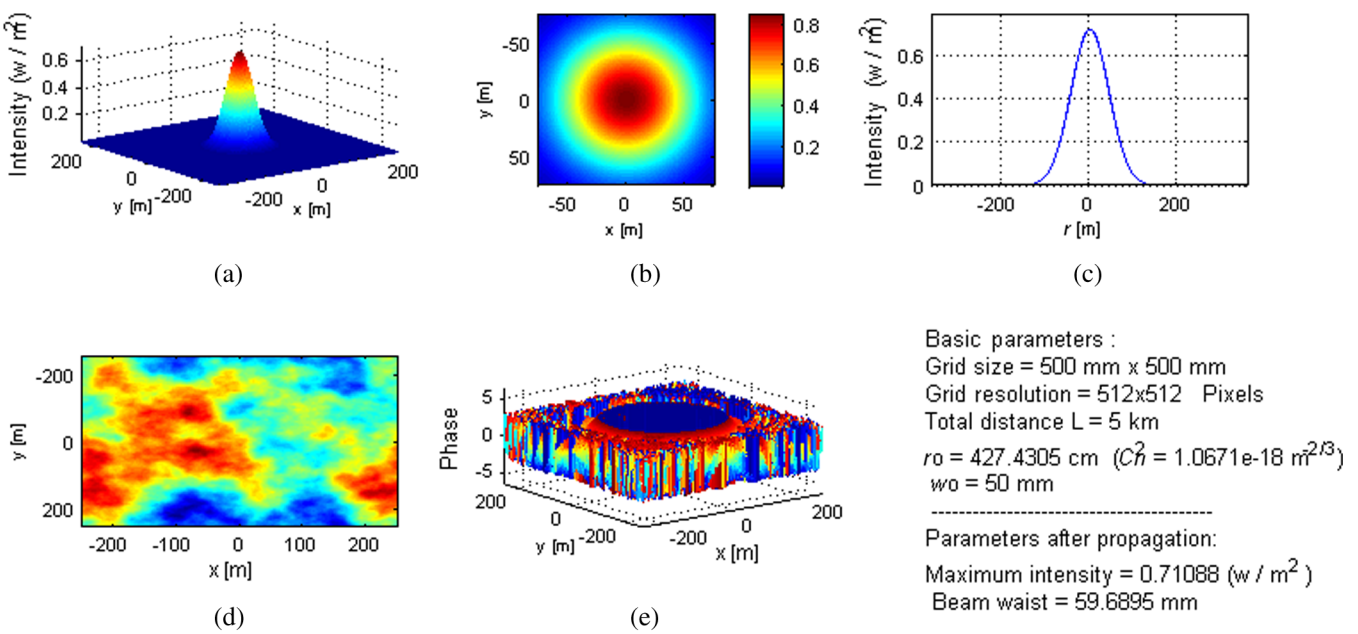

Fig. 3 Gaussian beam propagation to distance $z = L$ (phase screen at the object plane): (a) three-dimensional (3-D) Gaussian beam, (b) its transverse plane intensity distribution, (c) two-dimensional (2-D) intensity profile, (d) random phase screen distribution profile, and (e) 3-D field phase angle distribution.

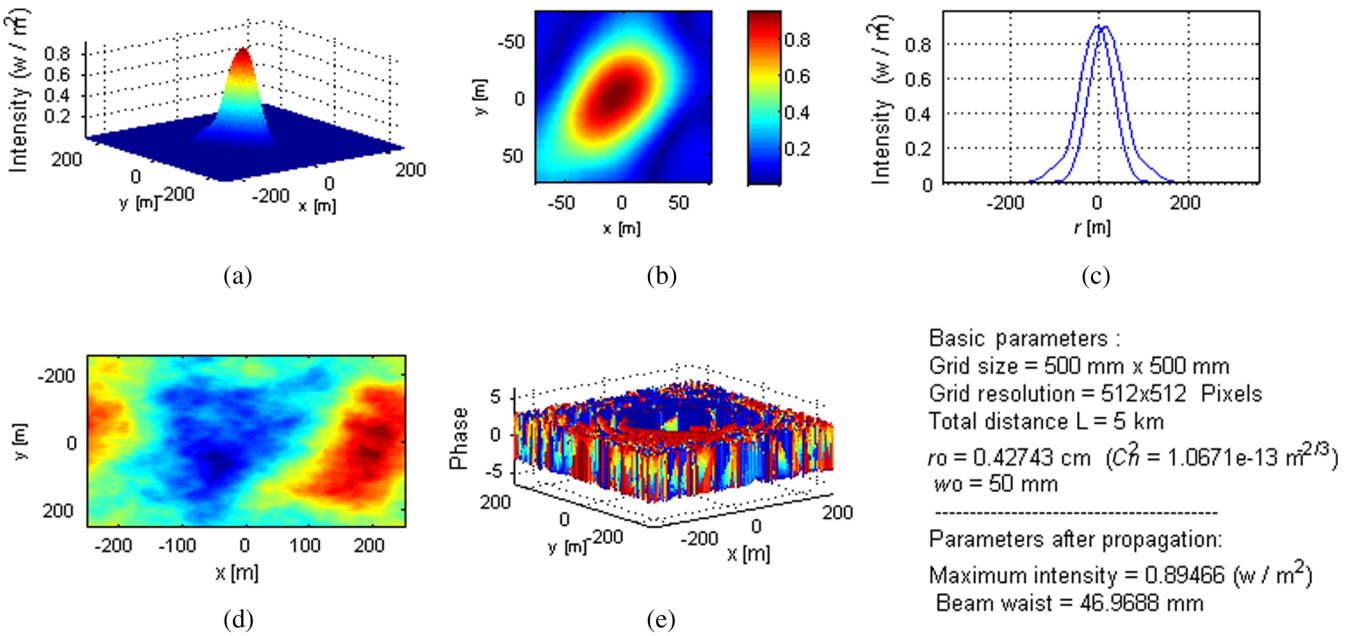

Fig. 4 Gaussian beam propagation to distance $z = L$ (phase screen at the object plane): (a) 3-D Gaussian beam, (b) its transverse plane intensity distribution, (c) 2-D intensity profile, (d) random phase screen distribution profile, and (e) 3-D field phase angle distribution. This plot involves strong turbulence and L = 5 km.

multiple phase screens. Of course the number of used phase screens is governed by the incremental distance Δz (preferably very small) and the propagation distance. The Gaussian beam 3-D view, its transverse plane intensity distribution, 2-D intensity profile, the random phase screen distribution profile, and the field phase angle distribution in 3-D are evaluated at $z = \Delta z$, $z = 0.5\ L$, and $z = L$ as illustrated in the following figures. We note here that ideally the split-step method requires that nonturbulent diffraction-limited propagation occurs between alternate phase screens, and thus in order to make this assumption mathematically viable, it is necessary that the interscreen distance Δz be infinitesimally small (i.e., $\Delta z \to 0$). In reality, however, it turns out that making Δz too small significantly increases the computation time. As a result, the values reported in this paper are based on optimal choices of Δz that yield reasonable results. Moreover, the values selected are compatible with those commonly used in the literature.

4.2.1 *Turbulence strength*

Because $\Delta z = 10$ m and $L = 5$ km, the number of random phase screens used is $n = 500$.

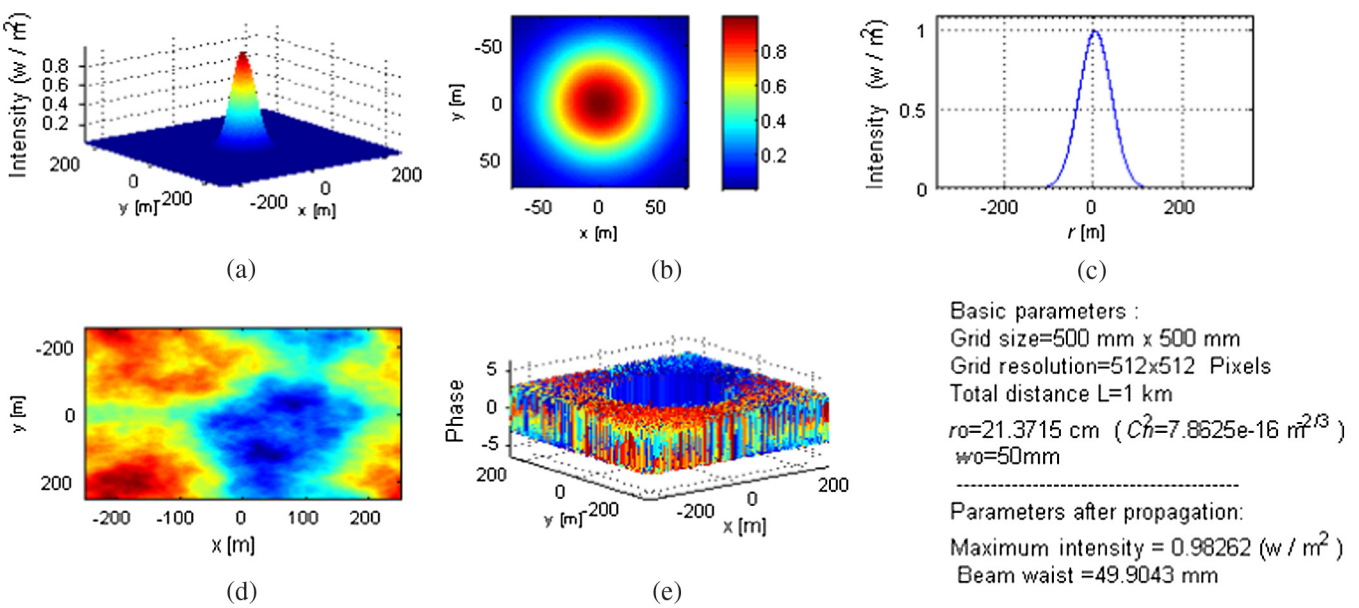

Fig. 5 Gaussian beam propagation to distance $z = L$ (phase screen at the object plane): (a) 3-D Gaussian beam, (b) its transverse plane intensity distribution, (c) 2-D intensity profile, (d) random phase screen distribution profile, and (e) 3-D field phase angle distribution.

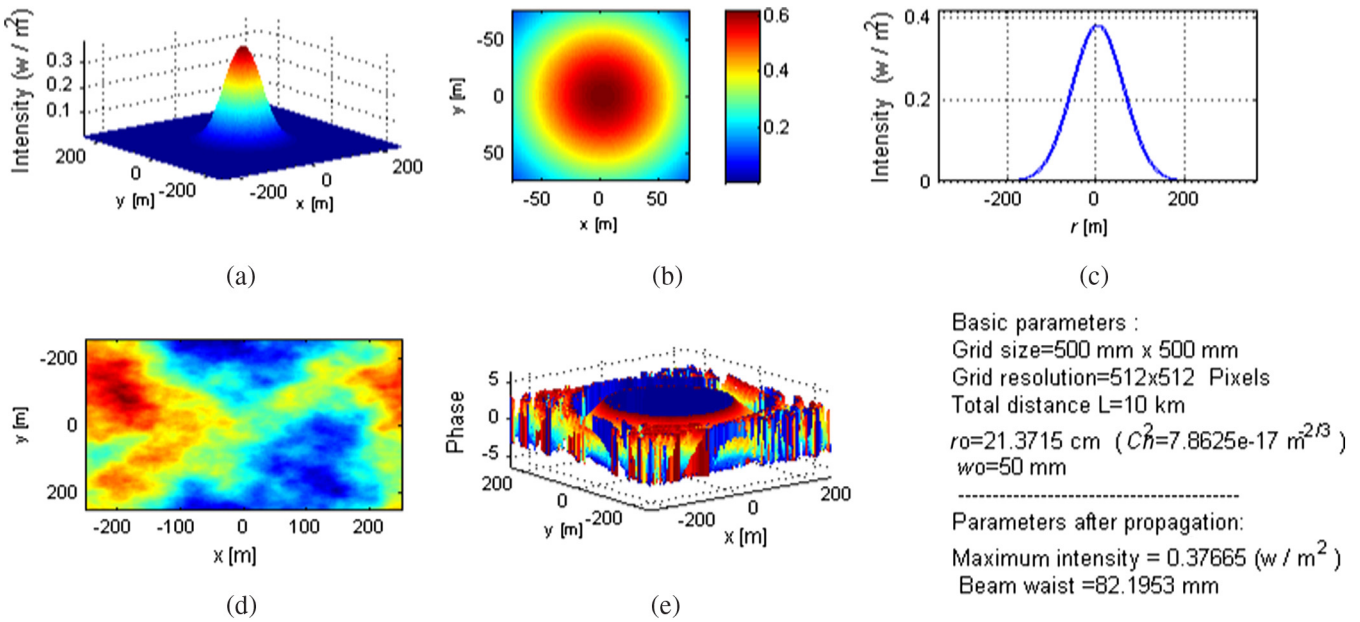

Fig. 6 Gaussian beam propagation to distance $z = L$ (phase screen at the object plane): (a) 3-D Gaussian beam, (b) its transverse plane intensity distribution, (c) 2-D intensity profile, (d) random phase screen distribution profile, and (e) 3-D field phase angle distribution. This plot involves moderate turbulence and L = 10 km.

(a) Weak turbulence ($r_0 = 10$ mm or $C_n^2 = 1.067 \times 10^{-18}$ m$^{-2/3}$)

(b) Strong turbulence ($r_0 = 0.01$ mm or $C_n^2 = 1.067 \times 10^{-13}$ m$^{-2/3}$)

From Figs. 7–9, we note that the transverse phase fluctuations increase as the propagation distance increases. In Fig. 7(e) when the beam characteristics are evaluated at the first increment), the phase fluctuations are concentrated mainly around the corners of the grid. Also, in Fig. 8(e) when the beam characteristics are evaluated halfway), the phase fluctuations become higher compared with the previous case. Following this trend, the maximum phase fluctuations occur when the field reaches image plane, as shown in Fig. 9(e). The corresponding peak field intensities drop from 1 W/m^2 (at $Z = \Delta z$) to 0.9 W/m^2 (at $Z = 0.5L$) and finally to 0.69 W/m^2 (at $Z = L$). These results also are in accord with intuition, as seen earlier. In the case of strong turbulence, the results are more dramatic for the extended turbulence problem than where seen for the corresponding narrow turbulence cases. This is evident from the plots in Figs. 10–12. Thus, we find severe profile distortion in the

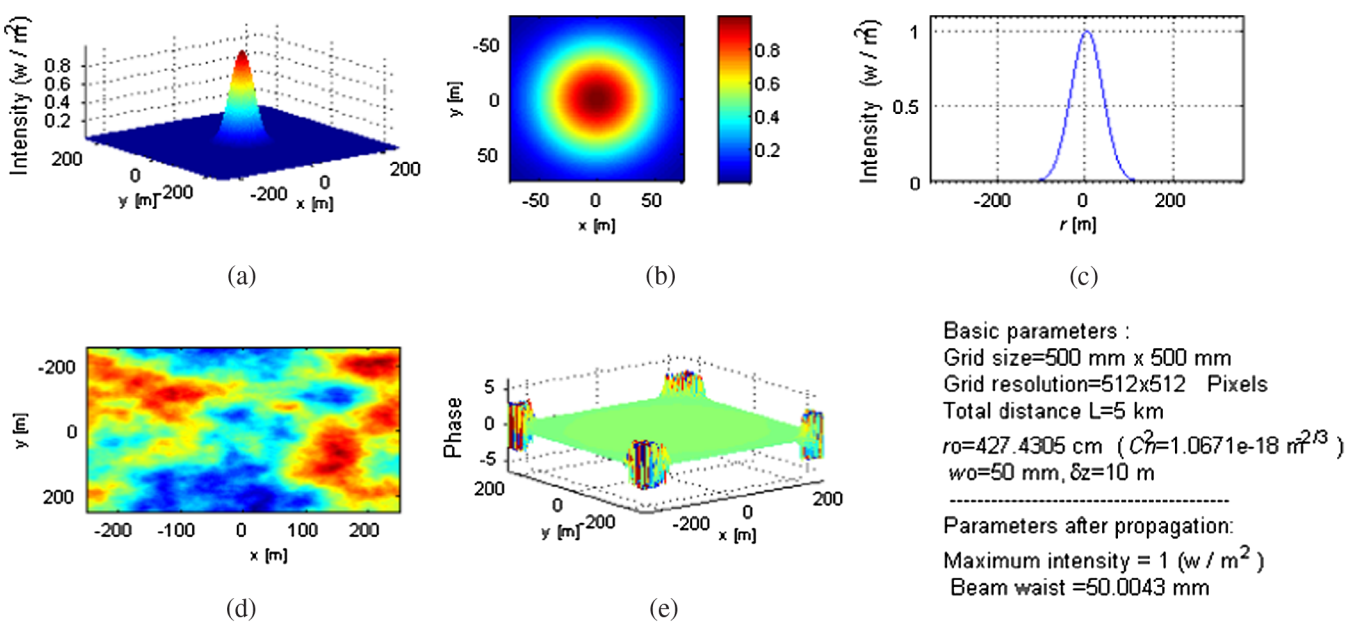

Fig. 7 Gaussian beam propagation to incremental distance Δz: (a) 3-D Gaussian beam, (b) its transverse plane intensity distribution, (c) 2-D intensity profile, (d) random phase screen distribution profile, and (e) 3-D field phase angle distribution.

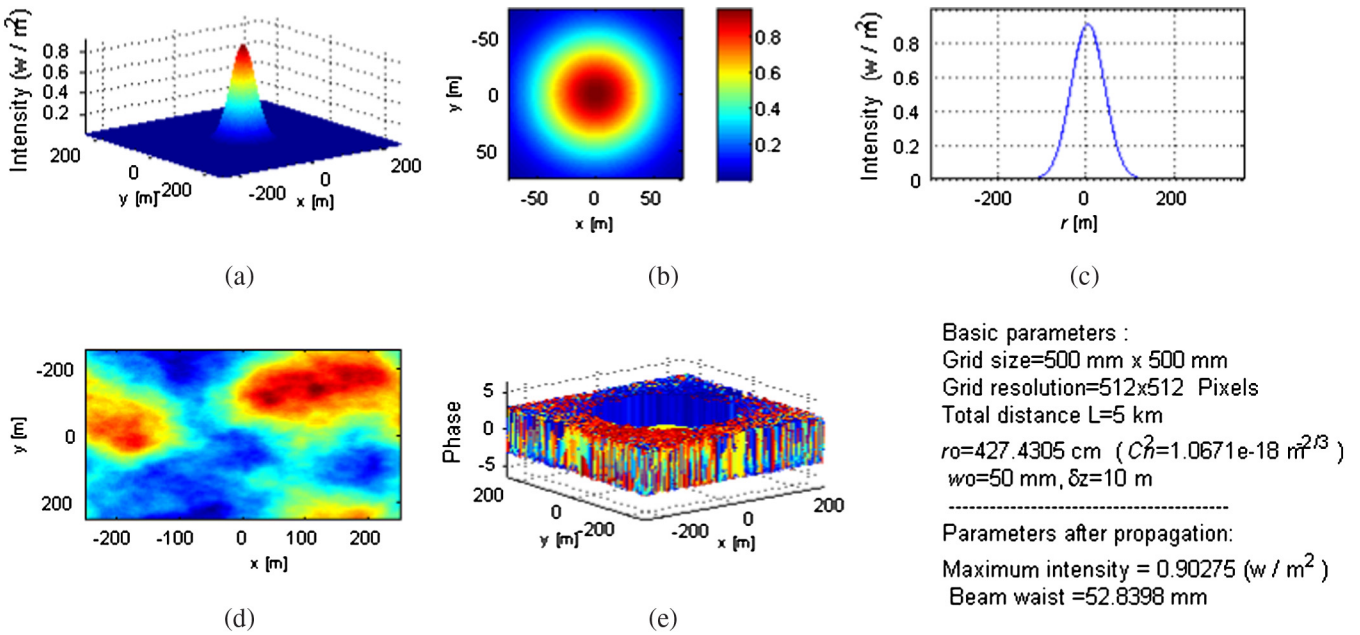

Fig. 8 Gaussian beam propagation to distance $Z = 0.5L$ (250 Δz): (a) 3-D Gaussian beam, (b) its transverse plane intensity distribution, (c) 2-D intensity profile, (d) random phase screen distribution profile, and (e) 3-D field phase angle distribution.

propagating beam already halfway along the path [Fig. 11(c)]. We observe multiple nested peaks that are spatially separated along with side lobes. Evidently, such beam splitting will have serious detection errors in any receiver system. At full propagation distance (Fig. 12), we find a complete breakdown of the original profile, and the received field therefore has an essentially scrambled profile [Fig. 12(c)]. These observations underscore the importance of studying beam propagation through (phase) turbulence, and the need for finding methods and strategies to minimize such distortions. Incidentally, numerical computations of the corresponding SI (presented later) further corroborate these findings in terms of the effects of both strong and more extended turbulence.

4.2.2 *Propagation distance (L)*

In this case, again we choose moderate turbulence ($r_0 = 0.5$ mm or $C_n^2 = 7.8625 \times 10^{-16}$ m$^{-2/3}$).

(a) $L = 1$ km

As $\Delta z = 10$ m, and $L = 1$ km, the number of random phase screens is $n = 100$ phase screens.

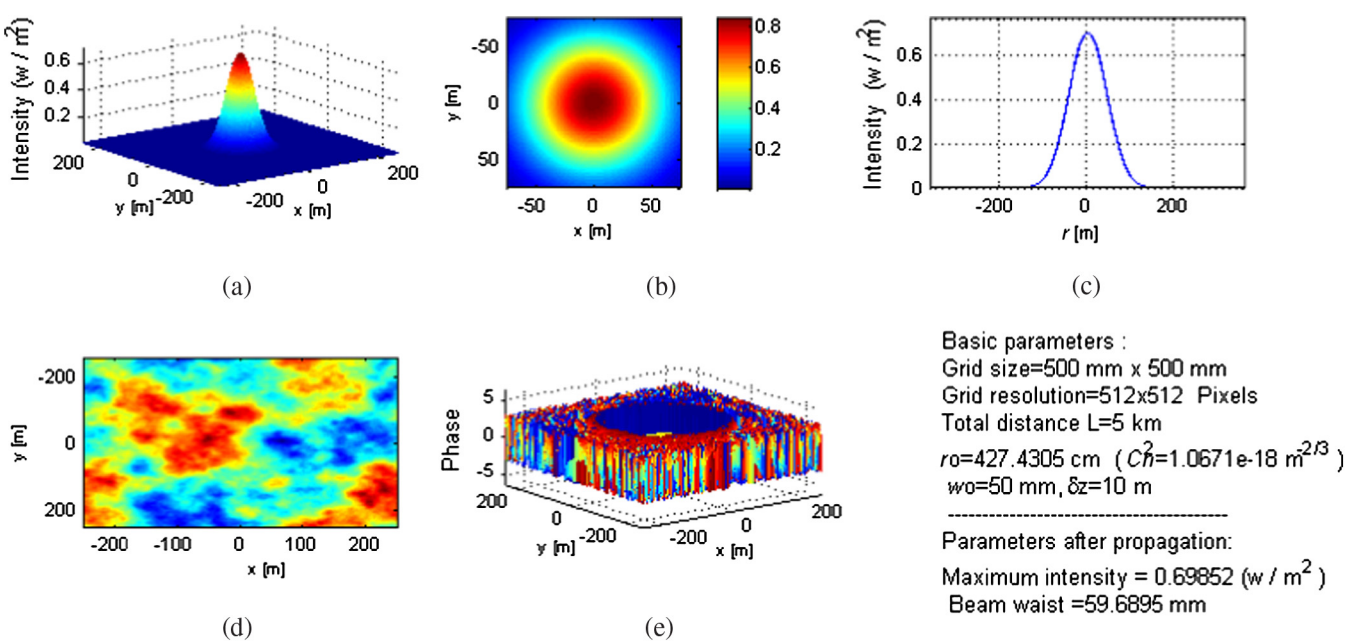

Fig. 9 Gaussian beam propagation to distance $Z = L$ (500 Δz): (a) 3-D Gaussian beam, (b) its transverse plane intensity distribution, (c) 2-D intensity profile, (d) random phase screen distribution profile, and (e) 3-D field phase angle distribution.

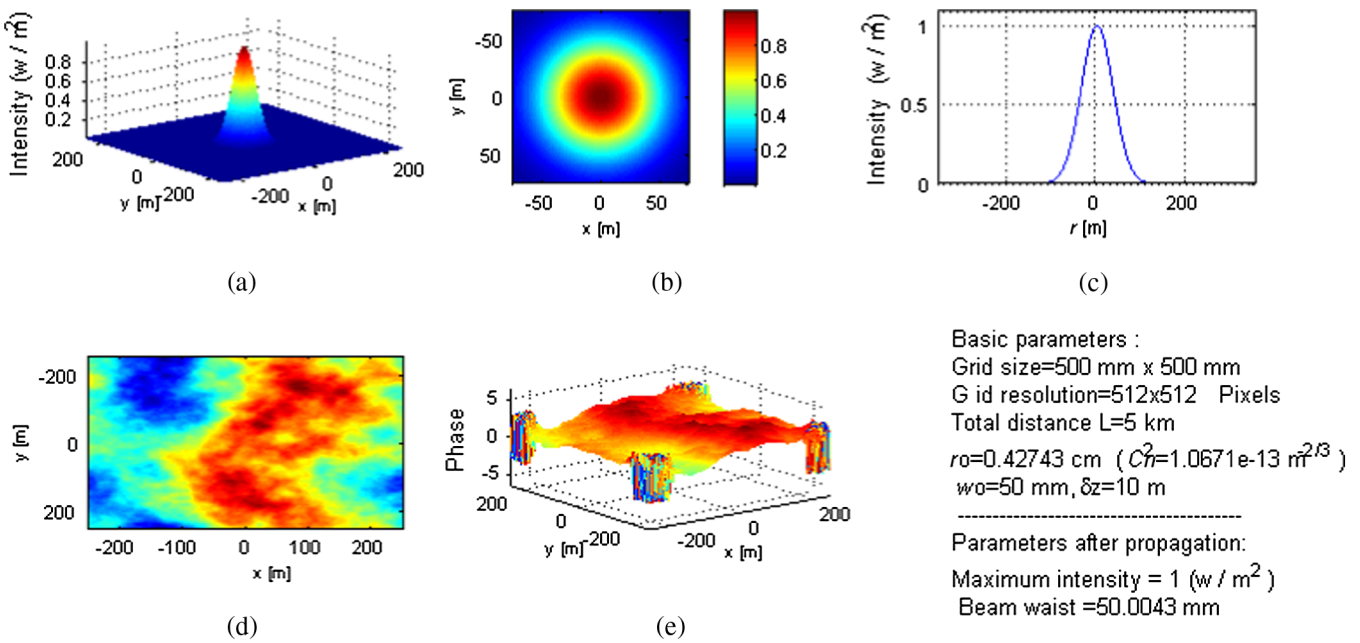

Fig. 10 Gaussian beam propagation to incremental distance Δz: (a) 3-D Gaussian beam, (b) its transverse plane intensity distribution, (c) 2-D intensity profile, (d) random phase screen distribution profile, and (e) 3-D field phase angle distribution.

(b) $L = 10$ km.

For $\Delta z = 10$ m, and $L = 10$ km, the number of random phase screens is 1,000.

We next note from Figs. 13 and 14 that the results are essentially identical regardless of the propagation distance (1 and 10 km) because the incident wave has traveled only to the distance Δz. We observe also that there is a tendency for phase fluctuations to accumulate near the corners of the grid at this stage. Although the exact reasons for this phenomenon are difficult to gauge, one might speculate that in the random computations, phase fluctuations likely accumulate beginning from the interior of the screen and becoming larger toward the edge. In terms of image processing, this may be compared with greater perturbations at higher spatial frequencies under high-pass behavior. When the propagation is examined at the halfway distances (as seen in Figs. 15 and 16), we find that there is a tendency

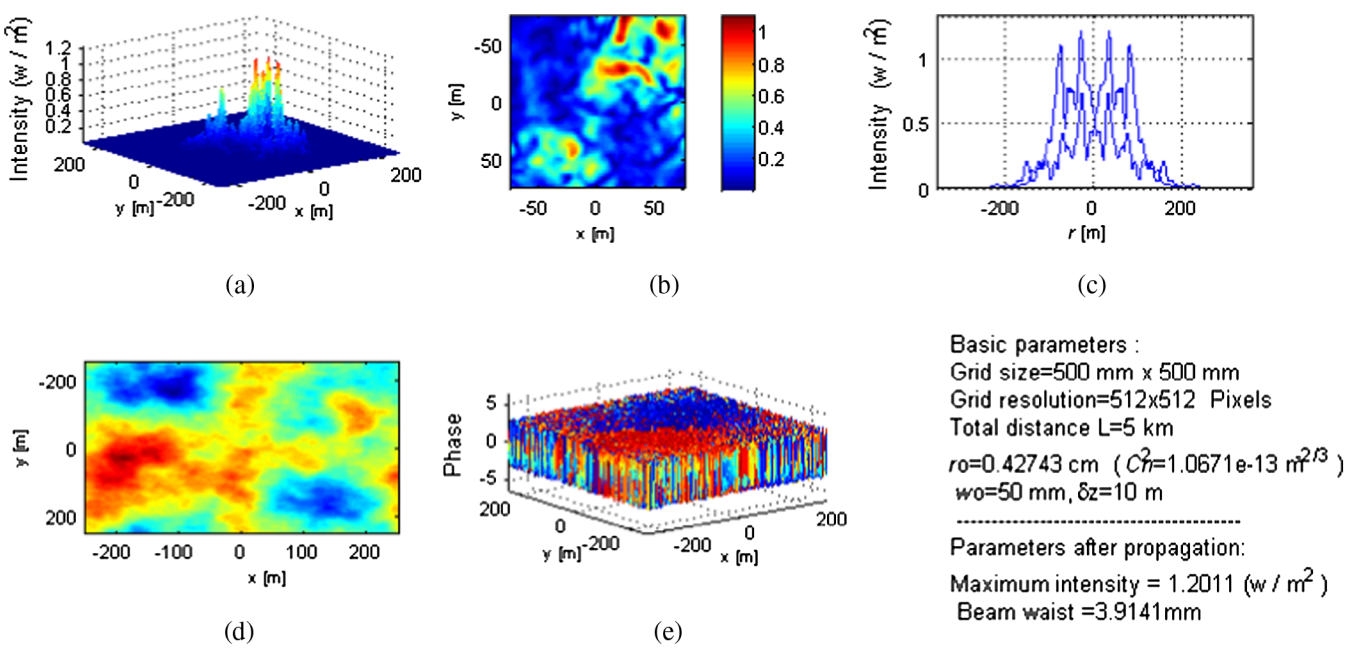

Fig. 11 Gaussian beam propagation to distance $Z = 0.5L$ (250 Δz): (a) 3-D Gaussian beam, (b) its transverse plane intensity distribution, (c) 2-D intensity profile, (d) random phase screen distribution profile, and (e) 3-D field phase angle distribution.

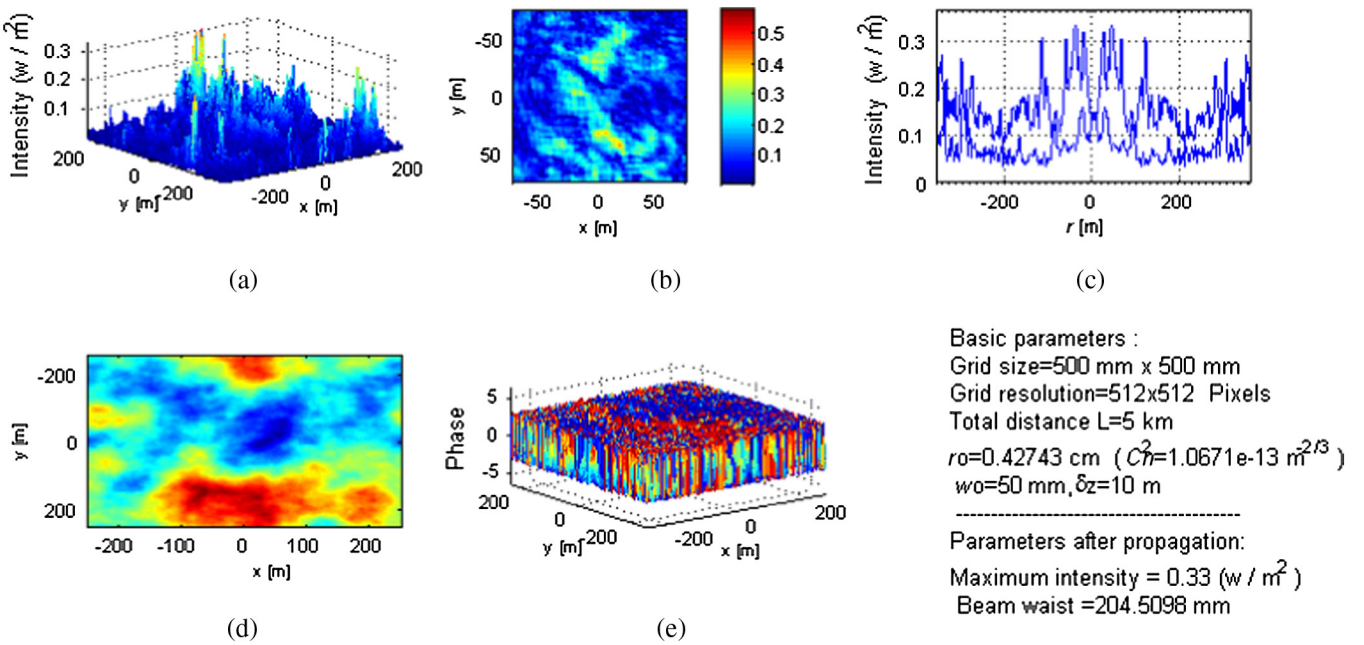

Fig. 12 Gaussian beam propagation to distance $Z = L\ (500\ \Delta z)$: (a) 3-D Gaussian beam, (b) its transverse plane intensity distribution, (c) 2-D intensity profile, (d) random phase screen distribution profile, and (e) 3-D field phase angle distribution.

toward beam-splitting (near the peak in Fig. 15 and also around the middle in Fig. 16) even for moderate turbulence, and additionally the beam is increasingly broadened as the propagation distance increases, accompanied by corresponding reductions in the peak intensity. These results corroborate intuition and expectation. At full propagation distance, we find that the incident beam undergoes highly visible beam-splitting (Figs. 17 and 18), and correspondingly, measurably higher broadening as well, up to 85 mm at a distance of 10 km (which closely matches the expected depth of focus of about 7.8 km for this diffraction problem). We observe also that beam intensity and profile measurements under weak or strong turbulence may also be numerically carried out using the methodology described above. Such results appear in the literature. For example, according to Ref. 11, the beam intensity profiles for increasing propagation distances tend to decay, as expected. Likewise, the profile widths for, say, Gaussian beams also diverge under turbulence

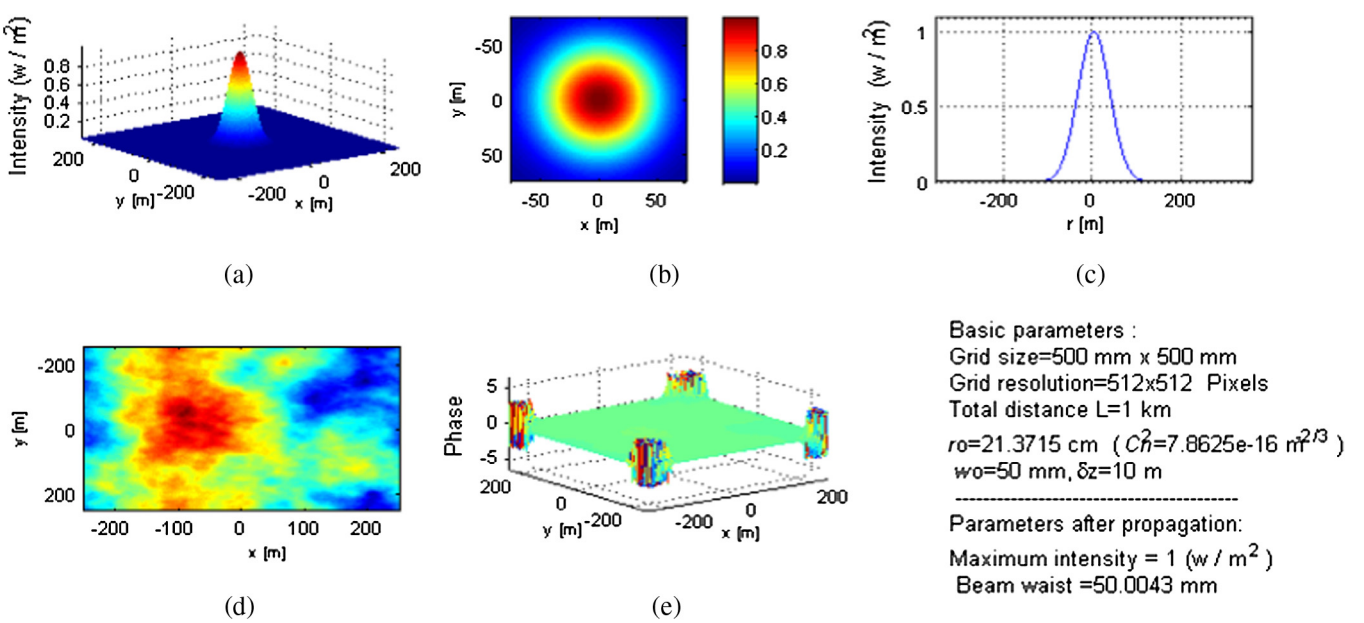

Fig. 13 Gaussian beam propagation to incremental distance Δz: (a) 3-D Gaussian beam, (b) its transverse plane intensity distribution, (c) 2-D intensity profile, (d) random phase screen distribution profile, and (e) 3-D field phase angle distribution.

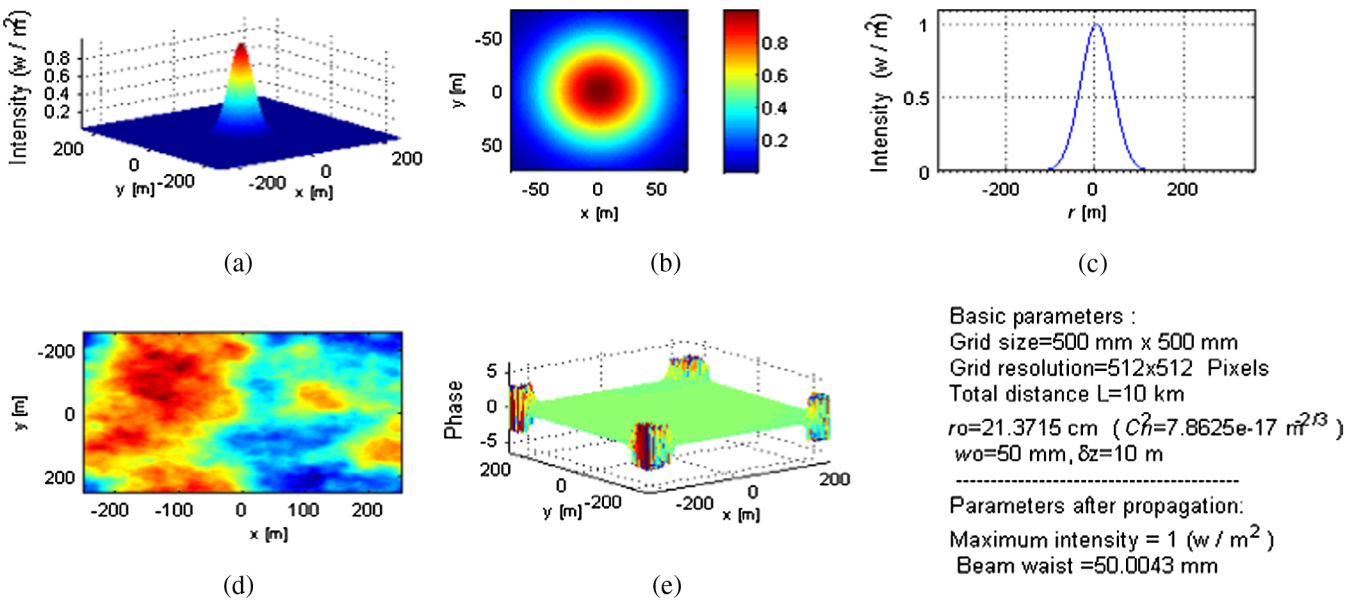

Fig. 14 Gaussian beam propagation to incremental distance Δz: (a) 3-D Gaussian beam, (b) its transverse plane intensity distribution, (c) 2-D intensity profile, (d) random phase screen distribution profile, and (e) 3-D field phase angle distribution.

compared with free-space. We note that the present work has analyzed both these properties with essentially the same results (not shown here).

4.2.3 *Incremental distance (Δz)*

In this case, once again we choose moderate turbulence ($r_0 = 0.5$ mm or $C_n^2 = 1.5725 \times 10^{-16}$ m$^{-2/3}$). As intuitively expected, the accuracy of the split-step algorithm requires the increment Δz to be arbitrarily small. However, as was discussed, making Δz too small increases the computation time considerably. In this section, we present two plots (measured at the full propagation distance) that clearly exemplify the effect of choosing smaller (versus larger) incremental distances in evaluating the overall propagation through turbulence with greater accuracy.

(a) $\Delta z = 1$ m

With $\Delta z = 1$ m, and $L = 5$ km, the number of random phase screens is 5,000 for this case.

We note that with the relatively small Δz chosen, the final beam profile exhibits much of the turbulence-induced splitting and phase behavior, as seen in Fig. 19.

(b) $\Delta z = 50$ m

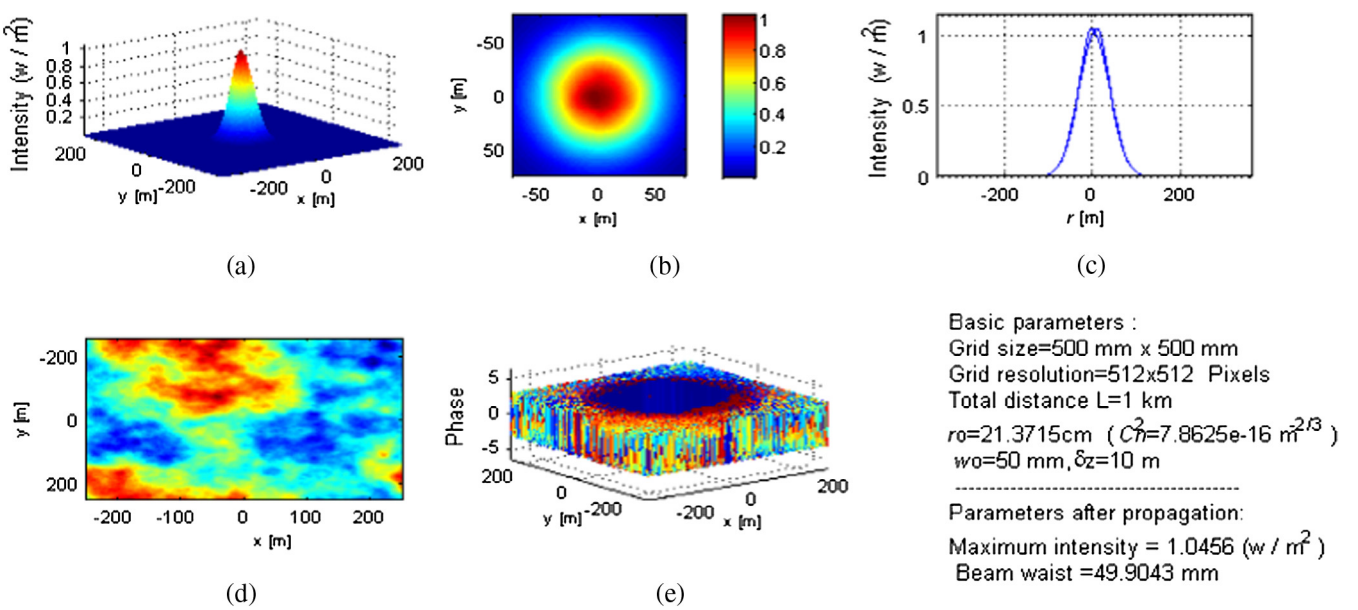

Fig. 15 Gaussian beam propagation to distance $Z = 0.5L$ (50 Δz): (a) 3-D Gaussian beam, (b) its transverse plane intensity distribution, (c) 2-D intensity profile, (d) random phase screen distribution profile, and (e) 3-D field phase angle distribution.

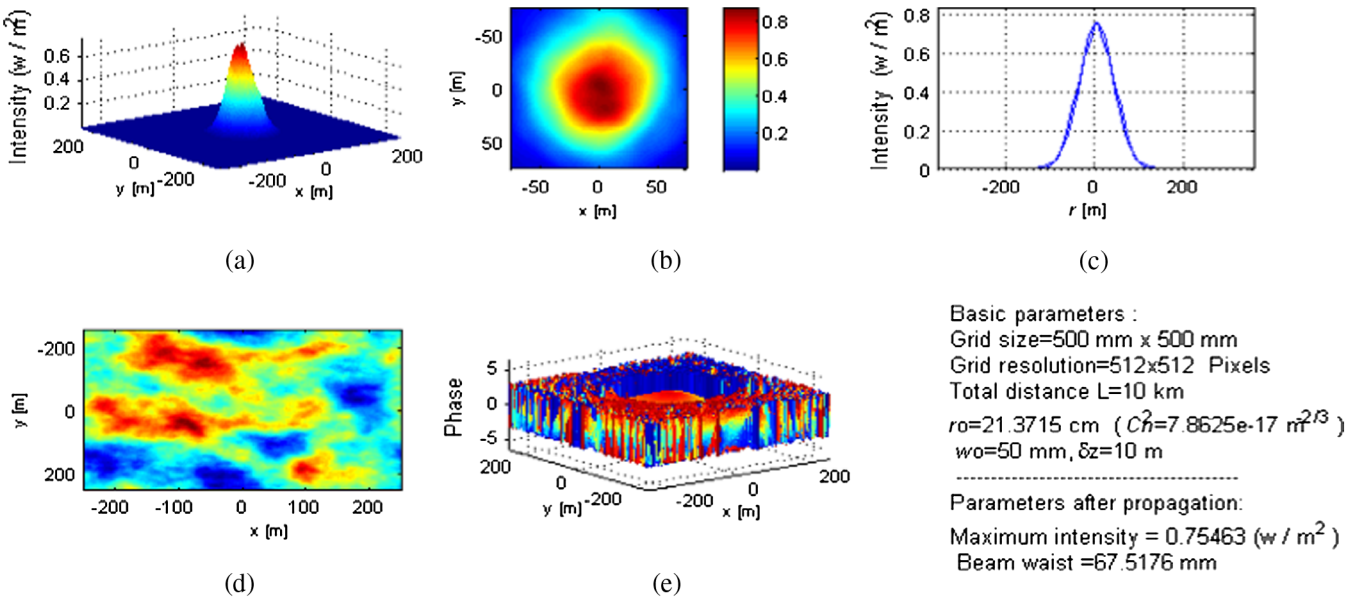

Fig. 16 Gaussian beam propagation to distance $Z = 0.5L$ (500 Δz): (a) 3-D Gaussian beam, (b) its transverse plane intensity distribution, (c) 2-D intensity profile, (d) random phase screen distribution profile, and (e) 3-D field phase angle distribution.

The number of random phase screens is 100 for the much larger Δz chosen for this case.

From Fig. 20, we note that even at full propagation distance, the diffracted profile under moderate turbulence exhibits only minimal amplitude (or intensity) splitting, a result which is obviously inaccurate when compared with the same propagation with a much smaller Δz, as seen in Fig. 19. As a final remark, we observe that in order to execute reliable numerical simulations via the split-step algorithm, there needs to be a tradeoff between accuracy and the acceptable computational time invested. Thus, it is very likely that by reducing the distance Δz even below 1 m, the accuracy gained may not justify the substantially higher computational time required.

4.3 *Scintillation Index with Extended Turbulence*

In this part, a single-Gaussian beam is propagated through extended phase turbulence, represented by a number of random phase screens. The corresponding SI is calculated at the image plane using Eq. (14). The beam width (w_0), Fried parameters (r_0), inner (ℓ_0), and outer (L_0) scales are all set to be constant during the propagation. Two turbulence conditions (weak and strong) are used in this subsection with results as follows:

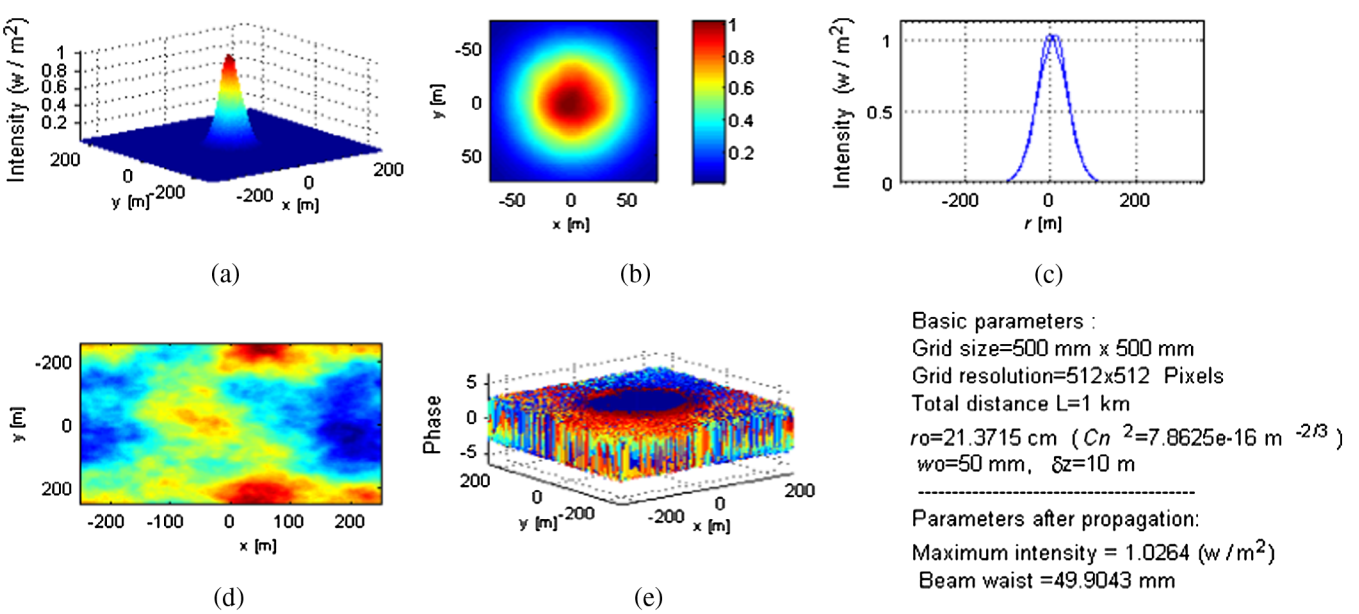

Fig. 17 Gaussian beam propagation to distance $Z = L$ (100 Δz): (a) 3-D Gaussian beam, (b) its transverse plane intensity distribution, (c) 2-D intensity profile, (d) random phase screen distribution profile, and (e) 3-D field phase angle distribution.

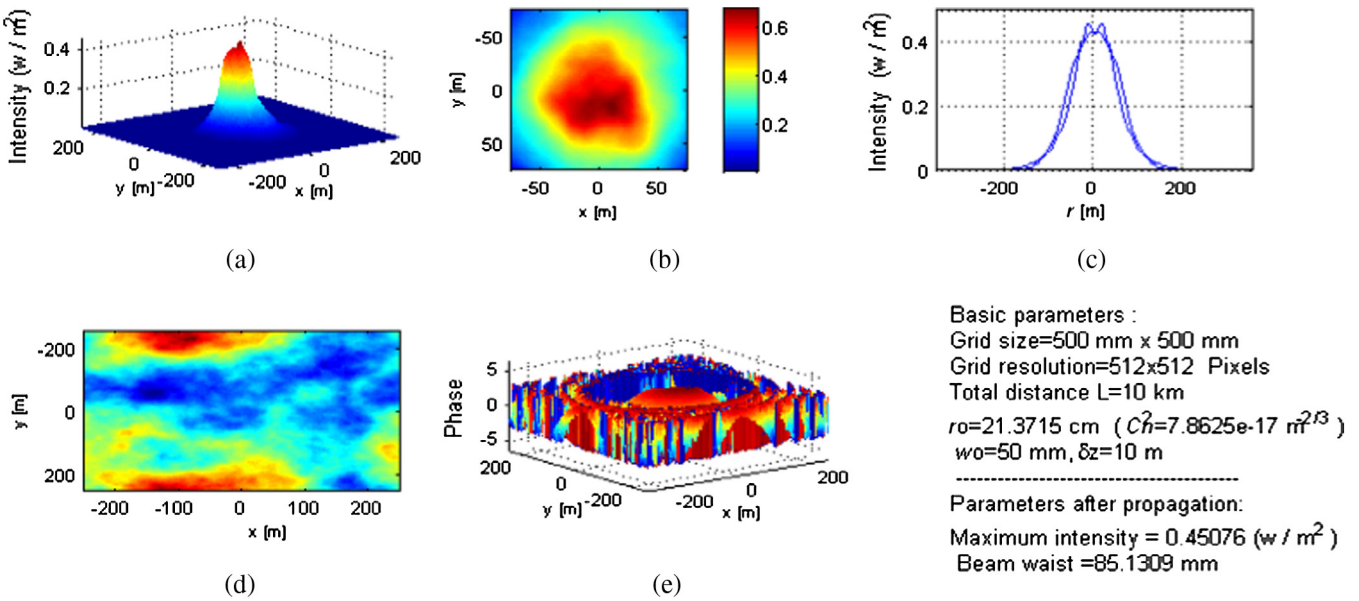

Fig. 18 Gaussian beam propagation to distance $Z = L$ (1000 Δz): (a) 3-D Gaussian beam, (b) its transverse plane intensity distribution, (c) 2-D intensity profile, (d) random phase screen distribution profile, and (e) 3-D field phase angle distribution.

(a) Weak turbulence ($C_n^2 \approx 10^{-18}$ m$^{-2/3}$)

Figure 21 shows the plot for the SI versus the number of phase screens for four different choices of propagation distance.

(b) Strong turbulence ($C_n^2 \approx 10^{-13}$ m$^{-2/3}$)

Once again, Fig. 22 shows the SI as a function of the number of phase screens corresponding to the same four propagation distances as in Fig. 21.

Generally, as expected, the SI increases with the propagation distance. Also, the SI increases in the case of strong turbulence compared with weak turbulence. An important observation here has to do with the asymptotic trends in the set of SI plots. We first note that in the case of weak turbulence (Fig. 21), the SI curve invariably rises up, but eventually appears to converge asymptotically toward a steady-state value. This trend is readily explained by the fact that as the number of phase screens (n) increases, the distance Δz goes down, thereby increasing the computational accuracy. As a result, below a threshold value of Δz, further increase in the number of phase screens will not enhance the accuracy (or the SI for these plots) appreciably, and therefore,

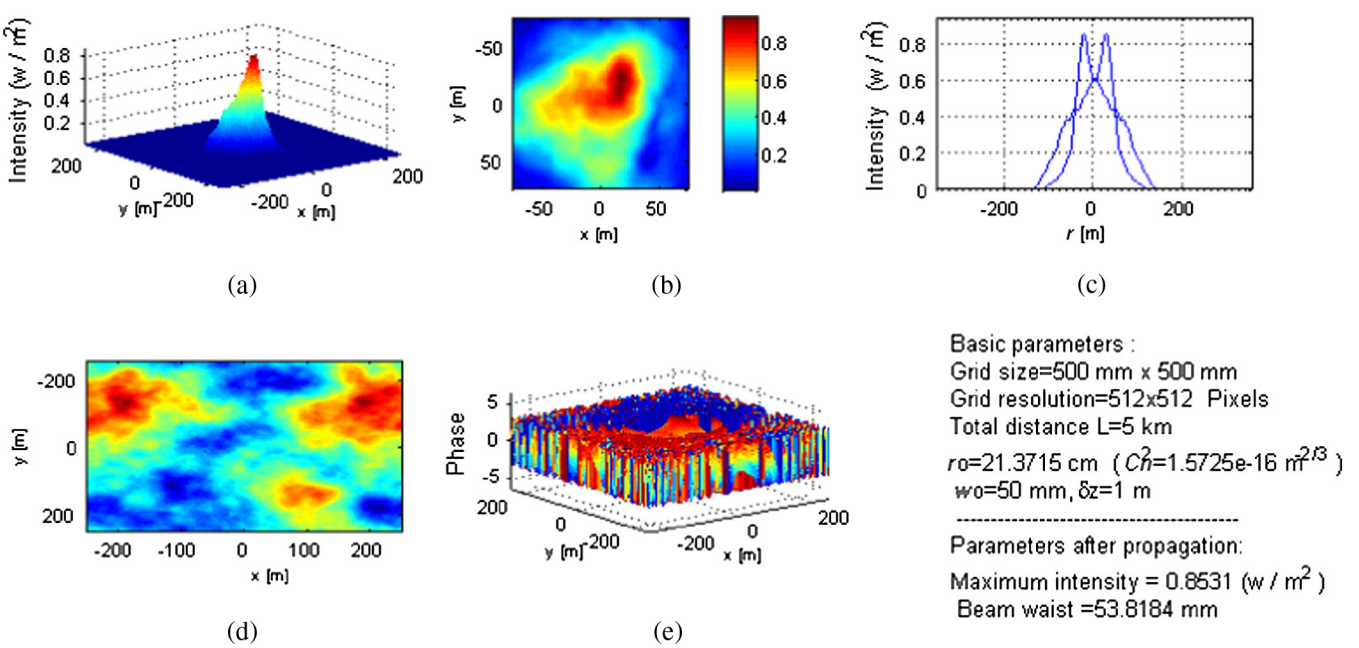

Fig. 19 Gaussian beam propagation to distance $Z = L$ (5000 Δz): (a) 3-D Gaussian beam, (b) its transverse plane intensity distribution, (c) 2-D intensity profile, (d) random phase screen distribution profile, and (e) 3-D field phase angle distribution.

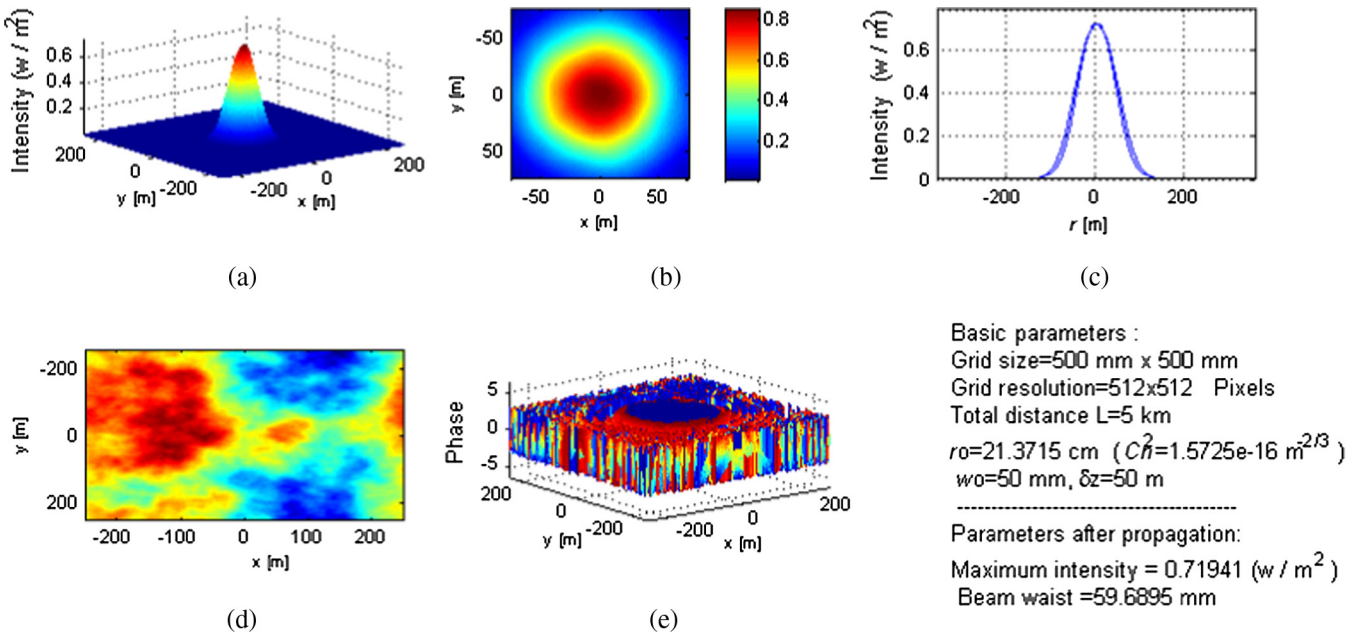

Fig. 20 Gaussian beam propagation to distance $Z = L$ (100 Δz): (a) 3-D Gaussian beam, (b) its transverse plane intensity distribution, (c) 2-D intensity profile, (d) random phase screen distribution profile, and (e) 3-D field phase angle distribution.

the graphs will converge to a steady-state. On the other hand, for strong turbulence, accuracy demands a much smaller Δz for similar parameter values as the weak turbulence case since greater beam fluctuations are expected. This trend is also observed in the plots of Fig. 21, where within a range of n of up to 100 (which is rather small from the accuracy perspective with strong turbulence), the SI curves continue to be on the rise. It is expected that if n were increased sufficiently, the curves would once again begin to saturate, indicating that an accuracy threshold for Δz has been reached. In Fig. 22, the SI has been plotted for strong turbulence corresponding to different propagation distances. We observe that the SI values for weak turbulence tend to saturate within a phase screen count of 100; on the other hand, the SI under strong turbulence is still on the rise for the same phase screen count. This implies that under strong turbulence, saturation of the SI requires greater phase screen

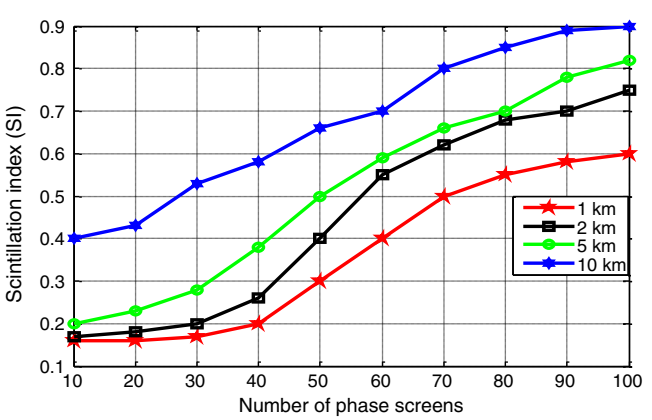

Fig. 21 The scintillation index plotted as a function of number of phase screens. The (constant) parameters are $w_0 = 30$ mm, $r_0 = 10$ mm, $\ell_0 = 10$ mm, and $L_0 = 1000$ mm. The propagation distance is given in the legend in kilometers.

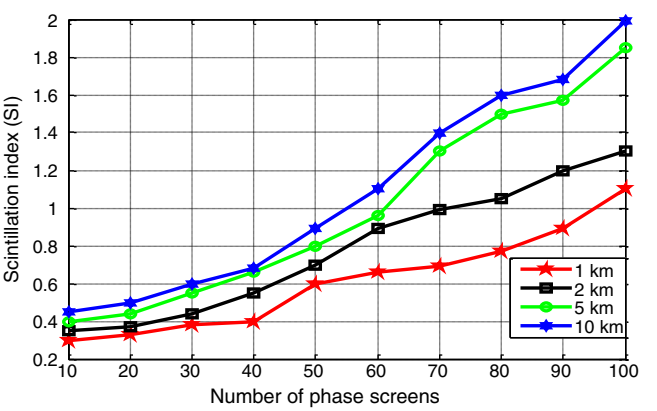

Fig. 22 The scintillation index plotted as a function of number of phase screens. The (constant) parameters are $w_0 = 30$ mm, $r_0 = 10$ mm, $\ell_0 = 10$ mm, and $L_0 = 1000$ mm. The propagation distance is given in the legend in kilometers.

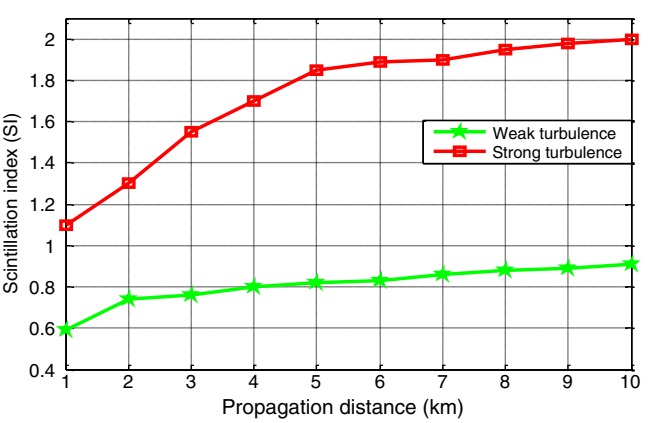

Fig. 23 The scintillation index plotted as a function of total propagation distance for weak and strong turbulence. The (constant) parameters are $w_0 = 30$ mm, $r_0 = 10$ mm, $\ell_0 = 10$ mm, $L_0 = 1{,}000$ mm, and the number of phase screens $n = 100$.

numbers (or, equivalently, much shorter screen placements). The SI values for strong turbulence are also consistently higher than those for the weak case. In several reports (as for example, in Panich et al.[20]), statistical measurements of scintillation characteristics caused by turbulence have been reported via theoretical and field measurements. One such is the SI of the scattering under turbulence, as reported in this paper. In Panich et al.,[20] measurements have been conducted for relatively strong turbulence ($C_n^2 = 1.3\times 10^{-13}$ m$^{-2/3}$) and at two different wavelengths. Of these, the case for 904 nm may be compared with the work reported here (at 1 μm). In view of this, the SI with MVKS turbulence in this work is plotted under strong turbulence ($C_n^2 \approx 10^{-13}$ m$^{-2/3}$), as shown in Fig. 23. According to Fig. 23, the value of SI at about 1 km is 1.1 under strong turbulence. From Ref. 20, the corresponding SI value at 903 nm around 1-km propagation distance is about 1.5. Thus, the two SI values compare favorably. A plot of SI in this paper corresponding to weak turbulence has also been shown in Fig. 23; it is expected that this would also be comparable with measured values in the literature.

4.4 *Fringe Visibility with Extended Turbulence*

By using two identical spatially separated Gaussian beams, the FV is determined using Eq. (15) at the observation plane for different values of propagation distance for a given number of random phase screens. The beam width (w_0), Fried parameters (r_0), inner (ℓ_0), outer (L_0) scales, and the separation distance between the two beams are all set to be

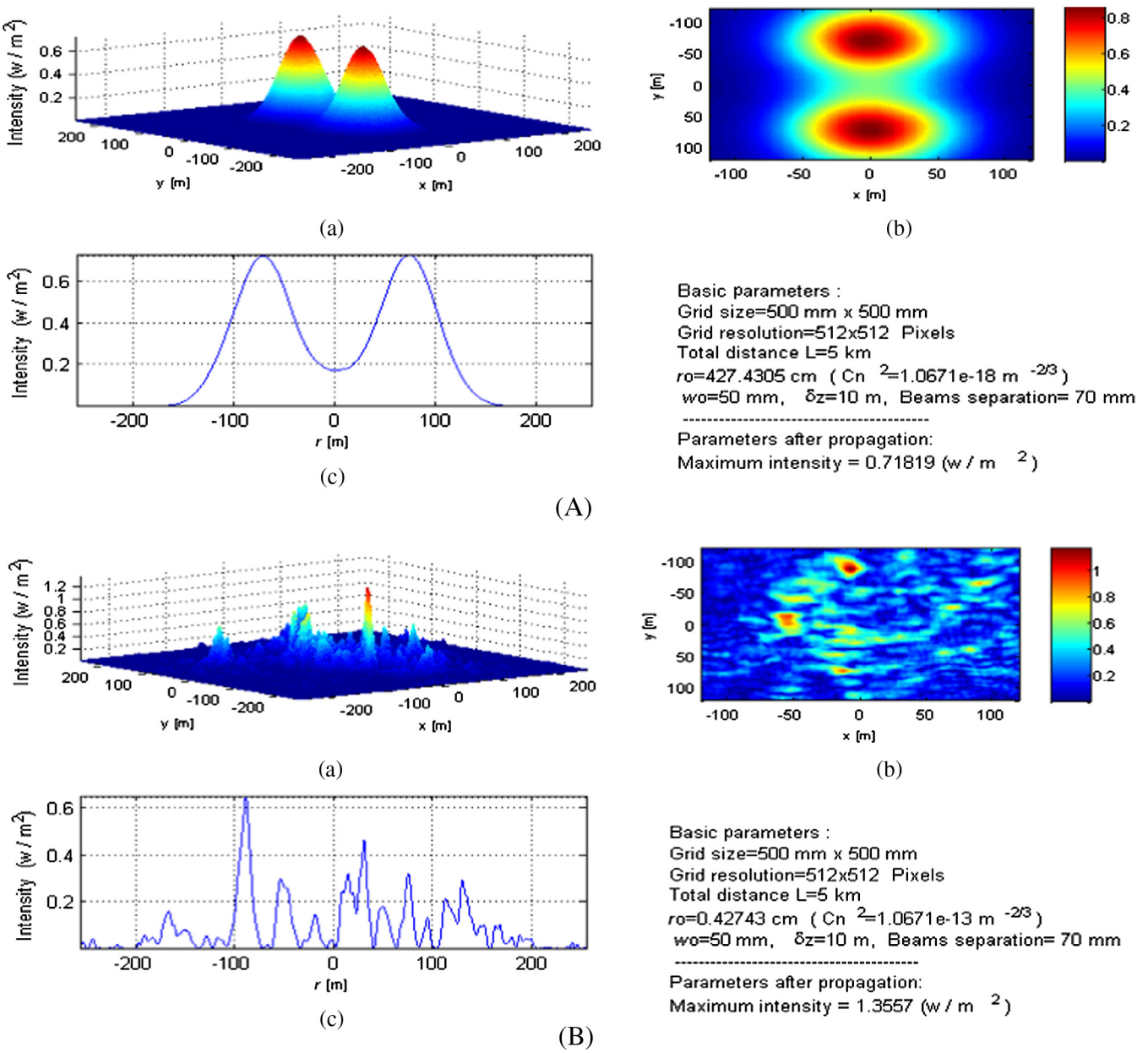

Fig. 24 (A) (a) Double Gaussian beam propagation to distance $Z = L$ through weak turbulence: (a) 3-D double Gaussian beam, (b) its transverse plane intensity distribution, (c) 2-D intensity profile. (B) Double Gaussian beam propagation to distance $Z = L$ through strong turbulence: (a) 3-D double Gaussian beam, (b) its transverse plane intensity distribution, (c) 2-D intensity profile.

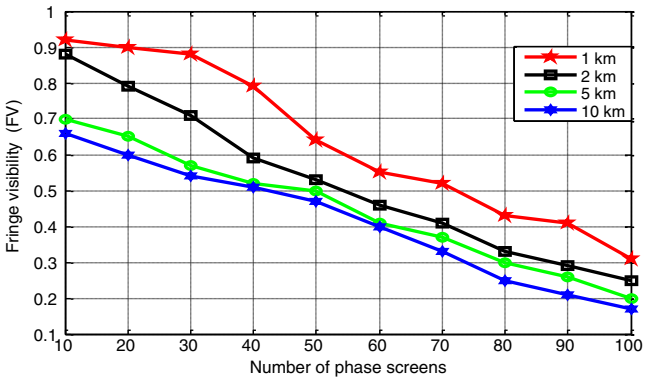

Fig. 25 The fringe visibility plotted as a function of number of phase screens. The parameters that held constant are $w_0 = 30$ mm, $r_0 = 10$ mm, beam separation = 70 mm, $\ell_0 = 10$ mm, and $L_0 = 1{,}000$ mm. The propagation distance is given in the legend in kilometers.

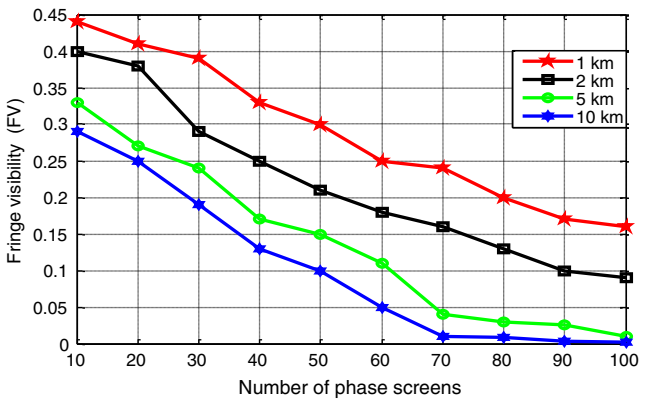

Fig. 26 The fringe visibility plotted as a function of number of phase screens. The parameters that held constant are $w_0 = 30$ mm, $r_0 = 10$ mm, beam separation = 70 mm, $\ell_0 = 10$ mm, and $L_0 = 1{,}000$ mm. The propagation distance is given in the legend in kilometers.

constant during the propagation. Again, in this simulation, weak and strong turbulence cases are considered to analyze the effect of the phase turbulence on the FV.

(a) Weak turbulence ($C_n^2 \approx 10^{-18}$ m$^{-2/3}$)
(b) Strong turbulence ($C_n^2 \approx 10^{-13}$ m$^{-2/3}$)

In Fig. 24, we show the overall profiles for double-Gaussian beams propagating through weak and strong turbulences [depicted by groups (A) and (B)]. As can be seen, in the presence of weak turbulence, there is marginal distortion in the received beam profile (an amplitude aliasing near the middle); however, the general features of the Gaussian are still visible. On the other hand, under strong turbulence, the received waveform is clearly distorted completely out of recognition.

From Figs. 25 and 26, in both cases (weak and strong turbulences), the FV decreases with the increasing of the propagation distance and with increasing of the number of phase screens. As expected, the FV has lower values in the case of strong turbulence compared with weak turbulence regime. Similar characteristics are seen in the work by Whitfield et al.;[3] clearly, these results show that stronger turbulence makes the diffraction patterns prone to more fluctuations, and consequently, leads to lower FV. As mentioned in the last subsection, the incremental distance (Δz) between the two adjacent phase screens can be calculated using the same procedure. Also, the simulation processing time increases as the propagation distance and the number of phase screens increase.

5 Concluding Remarks

In this work, we have studied the influence of the atmospheric turbulence upon profiled Gaussian beam propagation over arbitrary distances. A power spectral density (PSD) of the MVKS was used to represent the random behavior of the atmospheric turbulence via one or more random phase screen (s), which represent the phase fluctuations due to the refractive index variation in the turbulent medium. The numerical split-step propagational analysis approach is followed in order to track the evolution of the field along the propagation path by using the Fresnel–Kirchhoff diffraction integral within the (homogenous) medium and the random phase fluctuations within the turbulent (inhomogeneous) medium. In this paper, simulation results for narrow atmospheric turbulence with different turbulence conditions and propagation distances are reported briefly. In addition, propagation of profiled Gaussian beams through extended turbulence in relation to several parameters (varied individually) is presented in more detail. In this case, we have found that in order to replicate extended turbulence more accurately, the distance between the two adjacent random phase screens should be very small; on the other hand, using infinitesimally small incremental distances (Δz) for the computation leads to much higher complexity and needs considerably more processing time. To avoid unacceptably large computation times, a tradeoff between accuracy and processing time has been applied while ensuring reasonable results. The SI has been determined for the propagation of the Gaussian beam through both weak and strong turbulences. Finally, the FV has been calculated for the propagation of adjacent Gaussian beams through both weak and strong turbulences. Overall, the effect of strong turbulence on the profile and energy of the propagated beam (usually leading to serious distortion and loss of energy) is rather evident from all the simulations; on the other hand, propagation over longer turbulence regimes under moderate levels of turbulence appears to primarily affect the beam widths more than the profiles themselves. This investigation allows one to adequately track the random amplitudes and phases of profiled EM waves at an arbitrary output plane by use of the split-step technique and the MVKS modeling. In ongoing work, the strategies described above are used to develop medium PSDs for both atmospheric turbulence (MVKS at this time) and also AO chaos (not reported here) with the intent to finding the cumulative effect for propagation under a combination of both effects.

Acknowledgments

The authors would like to acknowledge extended discussions and advice from Dr. A. K. Majumdar (Department of the Navy) and Dr. P. P. Banerjee (University of Dayton). One of us (FM) would like to thank the Ministry of Higher Education, Government of Libya, for financial support toward this research.

References

1. X. Zhu and J. M. Kahn, "Free-space optical communication through atmospheric turbulence channels," *IEEE Trans. Commun.* **50**(08), 1293–1300 (2002).
2. V. S. Rao Gudimetlaa et al., "Phase screen simulations of laser propagation through non-Kolmogorov atmospheric turbulence," *Proc. SPIE* **8038**, 803808 (2011).
3. E. M. Whitfield, P. P. Banerjee, and J. W. Haus, "Propagation of Gaussian beams through a modified von Karman phase screen," *Proc. SPIE* **8517**, 85170P (2012).
4. L. C. Andrews, R. L. Phillips, and A. R. Weeks, "Propagation of a Gaussian-beam wave through a random phase screen," *Waves in Random Media (UK)* **7**, 229–244 (1997).
5. V. I. Tatarski, A. Ishimaru, and V. U. Zavorotny, *Wave Propagation in Random Media (Scintillation)*, SPIE Press, Bellingham, Washington (1992).
6. R. R. Kumar, A. Sampath, and P. Indumathi, "Secure optical communication using chaos," *Opt. Commun.* **4**(7), 773–778 (2011).
7. L. Larger and J. Goedgebuer, "Encryption using chaotic dynamics for optical tele-communications," *C. R. Physique* **5**, 609–611 (2004).
8. M. R. Chatterjee and M. Alsaedi, "Examination of chaotic signal encryption and recovery for Secure communication using hybrid acousto-optic feedback," *Opt. Eng.* **50**(5), 055002 (2011).
9. N. J. Corron, "A new approach to communications using chaotic signals," *IEEE Trans.* **44**(5), 373–382 (1997).
10. A. K. Majumdar, Department of the Navy, China Lake, California, Private Communication (2013).
11. C. D. V. Thomas and M. T. Clarke, "Scintillation of laser radiation due to Propagation through atmospheric turbulence, measurements, and theoretical calculations," *Proc. SPIE* **0369**, 557–563 (1983).
12. M. Vorontsov et al., "Wave optics of deep atmospheric turbulence: from underlying physics towards predictive modeling, mitigation and exploitation," AFOSR MURI Topic #12 (2010).
13. A. K. Majumdar and J. C. Ricklin, Eds., *Free-Space Laser Communications: Principles and Advances, Optical and Fiber Communications Reports*, Vol. 2, Springer, New York (2008).
14. L. C. Andrews and R. L. Phillips, *Laser Beam Propagation through Random Medium*, 2nd ed., SPIE Press, Bellingham, Washington (1998).
15. M. C. Roggemann and B. M. Welsh, *Imaging Through Turbulence*, CRC Press, Boca Raton, Florida (1996).
16. A. Ishimaru, *Wave Propagation and Scattering in Random Media*, Wiley-IEEE Press, New York (1997).
17. J. D. Schmidt, *Numerical Simulation of Optical Wave Propagation with Examples in Matlab*, SPIE Press, Bellingham, Washington (2010).
18. M. R. Chatterjee and F. H. A. Mohamed, "Investigation of chaotic profiled beam propagation through a turbulent layer and output temporal statistics using a modified von Karman phase screen," *Proc. SPIE* **8971**, 897102 (2014).
19. T. C. Poon and T. Kim, *Engineering Optics with Matlab*, World Scientific, Singapore (2006).
20. M. G. Panich et al., "Scintillation fluctuations of optical communication lasers in atmospheric turbulence," *Proc. SPIE* **9080**, 908013 (2014).

Monish R. Chatterjee has been a professor of electrical and computer engineering (ECE) at the University of Dayton since 2002. He has authored over 60 papers in archival journals and conference proceedings, several book chapters, four literary books, numerous literary essays, and presented over 100 papers at international conferences. He is a senior member of IEEE and OSA, a member of SPIE and Sigma Xi, and a fellow of the Golden Key National Honors Society.

Fathi H. A. Mohamed received his BSEE degree in communication engineering from the Higher Institute of Electronics, Bani-walid, Libya, in 1994, and the MSEE degree from Arab Academy for Science, Technology and Maritime Transport, Cairo, Egypt, 2005. He is currently completing his research for the PhD degree at the University of Dayton, Dayton, Ohio. His areas of research interests include acousto-optic, atmospheric turbulence, electromagnetic, and digital signal processing.